nature communications

Article

https://doi.org/10.1038/s41467-025-62175-1

Microbial responses to changing plant community protect peatland carbon stores during Holocene drying

Received: 12 February 2025

Accepted: 14 July 2025

Published online: 26 July 2025

Check for updates

Yiming Zhang[1,2,3], Xianyu Huang[1,2] ✉, Bingyan Zhao[1,4], Chaoyang Yan[2], Hongyan Zhao[5], Hongbin Zhang[1], Toby A. Halamka[3], Rebecca H. Peel[3], Mike Vreeken[3], Angela V. Gallego-Sala[6], Richard D. Pancost[3] & Shucheng Xie[1]

Peatlands are among the most effective long-term carbon sinks. However, climate change is triggering major ecological shifts with widespread woody plant expansion in peatlands. How microbial processes regulate carbon storage under these vegetation transitions remains uncertain. Here, we integrate multi-proxy records from a subtropical fen peatland in China with a global synthesis of paleoecological data from 155 peatlands to reveal a critical carbon regulation mechanism: woody expansion within peatlands can enhance long-term carbon storage by reshaping microbial metabolism and peat organic composition. We find mid-Holocene warming- and drying-driven woody encroachment displaced herbaceous plants, suppressing bacterial heterotrophy and shifting metabolism toward autotrophy. This transition coincides with peat organic matter transformations, marked by decreased carbohydrates and increased aromatics, promoting recalcitrant carbon pools. Together, this cascade of processes amplifies carbon accumulation, with peak rates occurring alongside diminished microbial heterotrophy during woody expansions. Our findings highlight key microbial responses to vegetation shifts that protect peatland carbon storage under climatic stress.

Peatlands cover only 3% of the global land but contain 500–700 Gt of carbon, accounting for around 30% of global soil carbon stocks[1,2]. They act as key carbon reservoirs that have been sequestering atmospheric carbon in peat deposits during the past millennia[3–5]. With intensified climate change and anthropogenic activity, peatlands are experiencing substantial ecological shifts, with widespread encroachment of woody plants such as shrubs and trees observed in many peatlands[6–10], driven by warming and lower water tables that favor shrub and tree root growth[11]. Woody plant expansion not only reduces *Sphagnum* mosses and herbaceous plants but also influences peat microbial metabolism[6,12], affecting carbon accumulation dynamics and the long-term balance between carbon storage and release. Yet, the long-term impacts of woody plant encroachment on carbon storage remain uncertain - a critical gap, as projections suggest intensified woody expansion in the coming decades[9,11]. Understanding how woody plant expansion shapes microbial communities, metabolic activity, and carbon dynamics in peatlands is therefore essential.

[1]State Key Laboratory of Geomicrobiology and Environmental Changes, China University of Geosciences, Wuhan, China. [2]Hubei Key Laboratory of Critical Zone Evolution, School of Geography and Information Engineering, China University of Geosciences, Wuhan, China. [3]Organic Geochemistry Unit, School of Chemistry, and School of Earth Sciences, University of Bristol, Bristol, UK. [4]Guangdong University of Petrochemical Technology, Maoming, China. [5]Key Laboratory of Geographical Processes and Ecological Security in Changbai Mountains, Ministry of Education, School of Geographical Sciences, Northeast Normal University, Changchun, China. [6]Department of Geography, University of Exeter, Exeter, UK. ✉e-mail: xyhuang@cug.edu.cn

Woody plant expansion influences peatland microbes by altering root exudates and litter chemistry[6,12]. As shown in field manipulation experiments, woody plant root exudates can stimulate peat microbial growth and production of carbon-degrading enzymes[6], causing ancient peat decomposition and increasing CO_2 emissions from peatlands[13]. A shift from *Sphagnum* to shrub has been shown to reduce bacterial diversity and increase dominance of a few keystone taxa, especially Acidobacteriota, suggesting an unstable belowground microbial community and potential degradation of peatlands[14]. In contrast, polyphenolic-rich woody litter suppresses microbial metabolism, slowing microbial decomposition and potentially enhancing carbon retention[12,15]. These contrasting effects suggest woody plant expansion has a dual and competing impact on microbial processes, necessitating further research to clarify its effect on peatland carbon stocks. However, studies of woody plant expansion typically focus on short-term impacts rather than the centennial-to-millennial scales essential for understanding long-term peatland carbon dynamics.

Peatlands have initiated and stored huge amounts of carbon since the Late Pleistocene, with peat deposits providing valuable records of long-term carbon accumulation as a balance of plant production and microbial decomposition[4,5,16]. Understanding these long-term carbon dynamics is crucial for predicting the future stability of these significant carbon stocks[16–19]. In peat deposits, plant macrofossils have been widely used to reconstruct historical vegetation changes[20] and reveal past shifts to woody plants that occurred in response to warm and dry periods[8,21,22]. Recent research documents ongoing woody expansion in circum-Arctic peatlands over the last 8000 years, often as a consequence of drier conditions[23]. However, linking these vegetation shifts with microbial activity and carbon accumulation over millennia remains challenging, as few records capture the integrated dynamics of plant community, microbial activity, and carbon storage across such long timescales.

In this study, we employ an integrated approach using multiple proxies from a southern Chinese peatland—Zhaogongting (ZGT) (Fig. 1) to explore how woody plant expansion and microbial interactions regulated carbon accumulation from the Late Pleistocene to the Holocene. Using plant macrofossils, we reconstructed plant community changes and identified significant mid-Holocene woody expansion events under drying conditions. Additionally, we analyzed bacterial lipid biomarkers, hopanoids, and their compound-specific carbon ($\delta^{13}C$) and hydrogen ($\delta^{2}H$) isotope compositions, as well as fungal-derived fatty acid biomarkers. The $\delta^{13}C$ and $\delta^{2}H$ isotopic profiles of these microbial lipids allow us to track shifts in microbial carbon cycling and metabolism[24–27]. Additionally, we determined the peat's carbon accumulation history and used Fourier Transform Infrared Spectroscopy (FTIR) and bulk geochemistry to analyze its organic matter composition, representing both its source and degradation, creating a framework that directly links vegetation, microbial activity, peat organic matter composition, and carbon accumulation dynamics. Our results demonstrate that woody plant expansion during the Holocene triggered significant fluctuations in bacterial and fungal biomass, carbon metabolism, and peat organic composition, with variations in heterotrophic activity closely tied to woody-driven changes in peat organic matter composition. The combination of transitions to recalcitrant organic matter pools and suppressed heterotrophic metabolism, resulted in the highest carbon accumulation rates observed from the Late Pleistocene to the Holocene, highlighting the critical role of microbial responses to changing plant community in enhancing peatland resilience and protecting long-term carbon storage under climate stress.

Results and discussion

Woody plant expansion during the Holocene

Plant macrofossils from the ZGT peat core reveal significant shifts in vegetation since the Late Pleistocene. Herbaceous plants and *Sphagnum* mosses dominated from the Late Pleistocene to the Early Holocene, accounting for roughly 80% of the total community, while woody plants comprised only about 20% (Fig. 2a). However, during the early mid-Holocene (8–6 ka), woody plant proportions increased dramatically in three phases, reaching nearly 90% (Fig. 2a). This interval also contains abundant *Sphagnum* (Fig. 2a), including two species, *S. palustre* and *S. subsecundum*, indicating that this had not become a forested swamp but a *Sphagnum* bog with a significant component of wood-forming shrubs and/or trees. After 6 ka, the proportion of woody plants stabilized back to around 20%, with herbaceous plants once again becoming dominant (Fig. 2a). Additional paleoecological studies from other peatlands in central-southern China, including Shuizhuyang, Daping, Shiwangutian, Dajiuhu, and Hongyuan, report increases in tree pollen percentages around 8 ka (Supplementary Fig. S1). These pollen records most likely reflect regional upland vegetation dynamics rather than local peat-forming communities within the peatlands. Therefore, while informative as regional background, we do not interpret them as evidence for a regionally synchronous expansion of woody plants across central-southern Chinese peatlands.

Our interpretation of woody plant expansion at the ZGT peatland is based on plant macrofossil evidence. However, our plant macrofossil reconstruction does not extend to the present due to data limitations. The uppermost peat layers are highly decomposed and compacted, making it difficult to recover well-preserved plant remains for reliable identification. Additionally, potential disturbances from modern land use may have affected the integrity of the surface peat record. Despite this limitation, our field surveys indicate that the modern ZGT peatland features a mix of shrubs (*Camellia caudata, Rhododendron* spp.), sedges (*Carex* spp.), and mosses (*Sphagnum palustre, Polytrichum commune*) (Fig. 1), suggesting that woody vegetation remains a component of the ecosystem but has not dominated as extensively as during the mid-Holocene expansion.

The mid-Holocene expansion of woody vegetation in the ZGT peatland appears to be tied to both warming and drying trends. Temperature reconstructions from the nearby Shuizhuyang peatland and Huguangyan Maar Lake, derived from branched glycerol dialkyl glycerol tetraethers, indicate a warming around 8 ka corresponding with the Holocene Thermal Maximum[28,29]. This warming trend, consistent with global Holocene patterns[30], likely supported woody plant expansion by promoting growth in warmer conditions, similar to the processes observed in circum-Arctic peatlands starting around 8 ka[23]. Modern studies also demonstrate that warming accelerates shrub and tree root growth, enabling woody plants to outcompete herbaceous vegetation in peatlands; for example, every degree increase in peat soil temperature has been shown to increase shrub fine root growth by 130%, providing shrubs with greater access to nutrients and water[11].

Local hydroclimatic changes also played a key role in driving woody plant expansion. In the ZGT peat core, $\delta^{13}C$ values of C_{29} and C_{31} *n*-alkanes show variability during the mid-Holocene, increasing by over 2‰ around 7–6 ka (Fig. 2b). However, this $\delta^{13}C$ change may result from both local hydrology and vegetation changes. To investigate, we analyzed $\delta^{13}C$ values of C_{29} and C_{31} *n*-alkanes from modern woody plants, herbaceous plants, and *Sphagnum* mosses in ZGT peatland, revealing significant differences among the three plant types, with woody plants having ~2‰ lower $\delta^{13}C$ values (Supplementary Fig. S2; Table S1). This suggests that woody expansion cannot account for the elevated $\delta^{13}C$ observed in the ZGT peat core. Instead, the elevated *n*-alkane $\delta^{13}C$ values may reflect reduced methanotrophy and/or enhanced water-use efficiency under drier conditions[26,31–34]. Our earlier analyses of $\delta^{2}H$ values of *n*-alkanes in the ZGT core show an overall increase from the early to late Holocene, indicating reduced moisture or drier conditions, albeit with particularly profound variability from 8 to 6 ka[35]. During the same interval, hopanoid flux also increased markedly (Fig. 2c), reflecting lower water tables and drier conditions in the

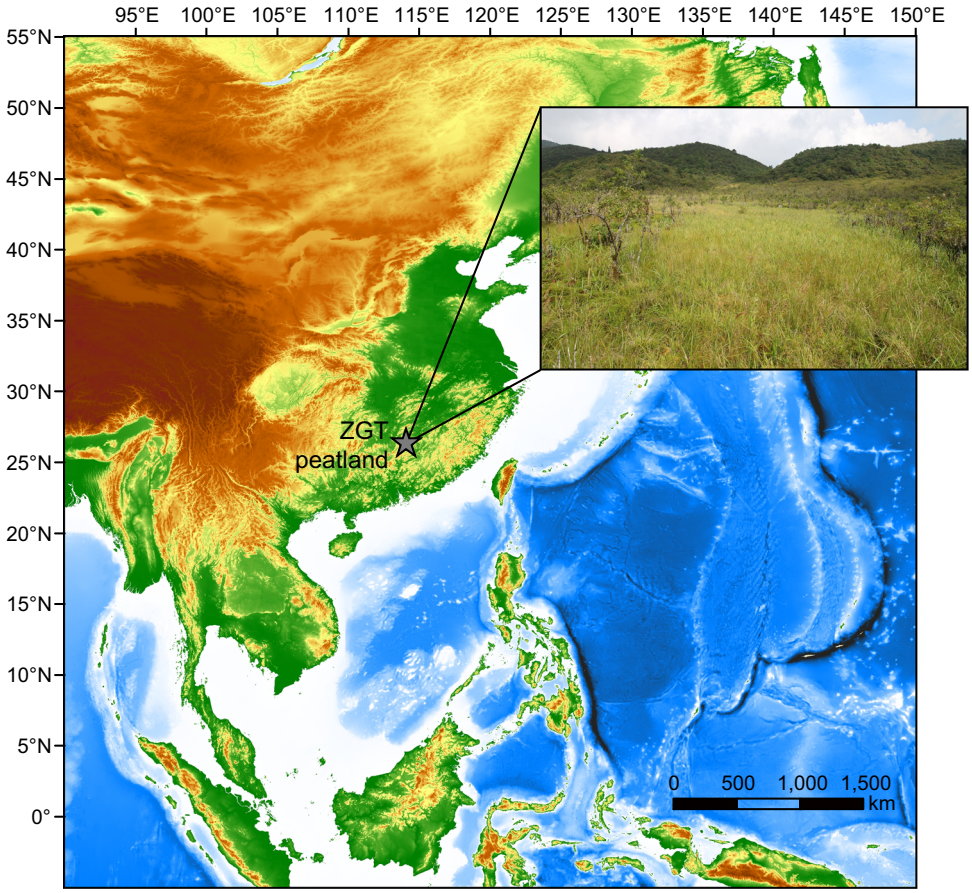

Fig. 1 | Site location and field photograph of ZGT peatland. The public elevation data are obtained from the USGS EROS Archive - Shuttle Radar Topography Mission (SRTM), provided by USGS/NASA (https://earthexplorer.usgs.gov). Field photograph taken in September 2016.

peatland[36]. This reduction in moisture availability contributed to drier conditions that facilitated woody plant encroachment. This phenomenon has been observed in peatlands in other areas of the world, where woody expansion was driven by drying and general water table drawdown[23,37,38]. In turn, the establishment of woody plants may further contribute to local drying through enhanced evapotranspiration and well-developed root systems[11,39], reinforcing the feedback between vegetation and peatland hydrology.

Microbial biomass and metabolism shifts during woody plant expansion

Hopanoid biomarkers in the ZGT peat core reflect dynamic bacterial responses to woody plant expansion between 8 and 6 ka (Fig. 2). Total concentrations of $C_{27}\beta$, $C_{29}\beta\alpha$, $C_{29}\beta\beta$, $C_{30}\beta\beta$, $C_{31}\alpha\beta$, and $C_{31}\beta\beta$ hopanes (where subscript refers to carbon number and Greek letters refer to stereochemistry at the C-17 and C-21 positions, respectively) initially increased, with a single-point peak around 7.3 ka (Fig. 2d); however, statistical analysis indicates no significant ($p = 0.40$, $t = 0.86$, $df = 25$, $n = 27$) difference in hopane concentrations between the 8–6 ka interval and other periods. The dominant $C_{31}\alpha\beta$ hopane, along with other hopanes such as $C_{29}\beta\alpha$ and $C_{30}\beta\beta$, followed similar trends, although others do not suggest a changing bacterial community throughout the entire record (Supplementary Fig. S3). While the isolated peak at 7.3 ka may reflect a short-term increase in bacterial biomass or hopanoid production under drier conditions[36,40,41], localized variability or analytical uncertainty cannot be excluded. Intriguingly, aside from the isolated peak at 7.3 ka, hopane concentrations show an overall decline relative to the early stage of the 8 ka interval, suggesting that putatively aerobic bacterial biomass decreased during the period of woody plant expansion (Fig. 2d and Supplementary Fig. S3), despite evidence for persistently dry conditions. This decline in bacterial biomass likely results from the continuous accumulation of lignin-rich woody residues, which reduce resources for bacterial growth and metabolism[12].

Similarly, the fungal biomarker $C_{18:2\omega6,9}$ fatty acid (where subscript 18 refers to carbon number, the colon and the number 2 indicate two double bonds, while ω and the numbers 6,9 indicate the positions of the double bonds) in the ZGT peat core exhibited an initial increase followed by a gradual decline during the woody plant expansion period. The concentration of $C_{18:2\omega6,9}$ fatty acid sharply increased around 8 ka (Fig. 2e), indicating a rapid rise in fungal abundance coinciding with the onset of local drying. This response likely reflects the stimulation of fungal growth under drier conditions, due to enhanced soil aeration and increased fungal metabolism[41]. Intriguingly, after 8 ka, the concentration of $C_{18:2\omega6,9}$ fatty acid gradually declined (Fig. 2e), indicating a decrease in fungal abundance despite the continued presence of dry conditions. This decline likely reflects a fungal adaptation to the progressive accumulation of phenolic-rich woody residues. For example, in shrub-dominated peatlands, fast-growing fungi are found to be suppressed and replaced by slow-growing taxa adapted to phenolic and recalcitrant substrates[15]. Therefore, our findings further highlight the inhibitory effect of woody plant expansion on fungal growth in peatlands over millennial timescales during the Holocene.

In addition to biomass, the $\delta^{13}C$ and $\delta^{2}H$ values of bacterial hopanoids in our ZGT core suggest shifts in bacterial carbon sources and metabolism during woody plant expansion. The $\delta^{13}C$ of the dominant $C_{31}\alpha\beta$ hopane exhibited considerable variation between −24‰ and −32‰ during the 8–6 ka period (Fig. 2f), with similar fluctuations observed for $C_{27}\beta$ and $C_{30}\beta\beta$ hopanes (Supplementary

https://doi.org/10.1038/s41467-025-62175-1

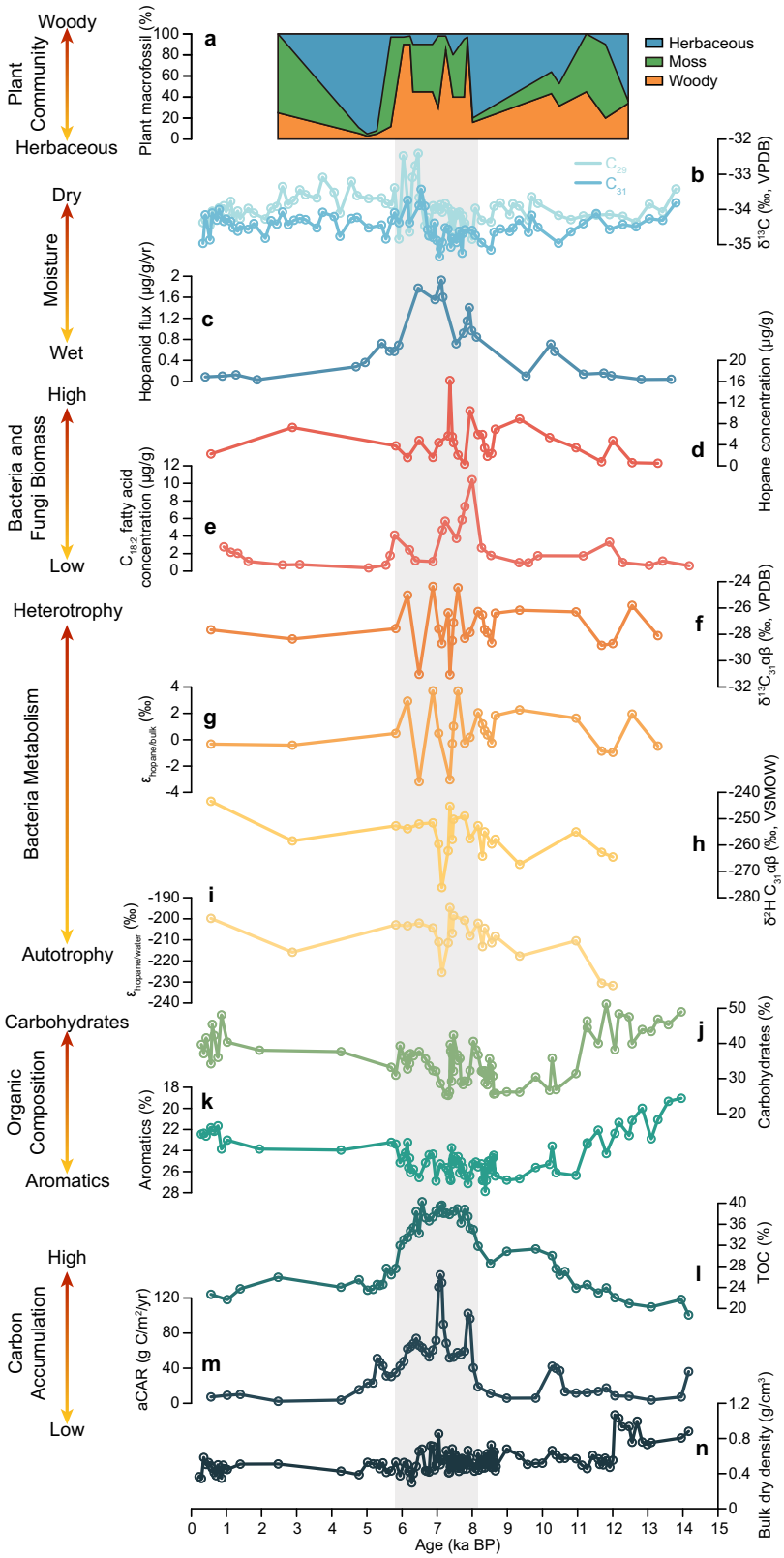

Fig. 2 | Holocene shifts in vegetation, microorganisms, peat organic composition, and carbon accumulation in ZGT peatland. a Proportion of plant macrofossils. **b** $\delta^{13}C$ values of C_{29} and C_{31} *n*-alkanes. **c** Hopanoid flux[35]. **d** Total concentration of bacterial $C_{27}\beta$, $C_{29}\beta\alpha$, $C_{29}\beta\beta$, $C_{30}\beta\beta$, $C_{31}\alpha\beta$, and $C_{31}\beta\beta$ hopanes. **e** Concentration of fungal $C_{18:2\omega6,9}$ fatty acid. **f** $\delta^{13}C$ of $C_{31}\alpha\beta$ hopane. **g** The carbon isotope offset ($\varepsilon_{hopane/bulk}$) between $\delta^{13}C$ of $C_{31}\alpha\beta$ hopane and bulk organic carbon. **h** $\delta^{2}H$ of $C_{31}\alpha\beta$ hopane. **i** The hydrogen isotope fractionation ($\varepsilon_{hopane/water}$) between $C_{31}\alpha\beta$ hopane and source precipitation water. **j** Proportion of carbohydrates. **k** Proportion of aromatics. **l** Total organic carbon content[35]. **m** Apparent carbon accumulation rate (aCAR)[35]. **n** Bulk density[35]. The gray shading marks the 8–6 ka period of woody plant expansion.

Fig. S4). In contrast, the $\delta^{13}C$ of bulk peat organic carbon ($\delta^{13}C_{bulk}$) remained stable (Supplementary Fig. S4). As a result, the offset between the $\delta^{13}C$ of $C_{31}\alpha\beta$ hopane and bulk organic carbon, $\varepsilon_{hopane/bulk}$, varied between −4 and 4‰ (Fig. 2g), suggesting a change in bacterial carbon source and/or metabolism during woody plant expansion. This may reflect a shift between ^{13}C-enriched substrates (e.g., sugars) and ^{13}C-depleted substrates (e.g., respired CO_2 or methane), and/or a transition between heterotrophy and autotrophy/methanotrophy[24,26,42,43].

The $\delta^{13}C$ values of C_{18} fatty acid also fluctuated markedly during the 8–6 ka interval, ranging from −30.8‰ to −24.7‰ (Supplementary Fig. S4). On average, these values (avg. −26.7‰) were ~1.5‰ more enriched than both bulk organic carbon and bacterial hopanoids (avg. −28.0‰), potentially indicating that microbes producing C_{18} fatty acids preferentially utilized ^{13}C-enriched substrates (e.g., sugars). Given that saturated C_{18} fatty acids can originate from fungi, bacteria, and higher plants, the observed $\delta^{13}C$ values likely reflect a combination of microbial and plant-derived carbon sources. While source attribution remains uncertain, the enriched values could reflect fungal contributions and support the interpretation of altered microbial metabolism during woody plant expansion under drier conditions.

The $\delta^{2}H$ values of the bacterial hopane also reveal dynamic metabolic behavior during woody plant expansion, although with different patterns than those of the $\delta^{13}C$ values. $\delta^{2}H$ values of the $C_{31}\alpha\beta$ hopane—for which we obtained the highest resolution record—generally increase from the early to late Holocene, with the major shift occurring from 8 to 6 ka and paralleling trends in *n*-alkane $\delta^{2}H$ values, albeit with a smaller magnitude. However, this trend is punctuated by a dramatic perturbation in the woody interval, with hopane $\delta^{2}H$ values initially increasing from −260‰ to −240‰ from 8 to 7 ka before sharply decreasing to −280‰ around 7.0 ka and then rebounding to −250‰ (Fig. 2h). These shifts could relate to changes in the $\delta^{2}H$ of source precipitation water, especially during hydroclimatic transitions. To eliminate source water $\delta^{2}H$ variability, we calculated the $\varepsilon_{hopane/water}$ value, representing hydrogen isotope fractionation between bacterial $C_{31}\alpha\beta$ hopane and precipitation water. Even after accounting for source water $\delta^{2}H$ changes, $\varepsilon_{hopane/water}$ values still showed considerable variation, rising from −210‰ to −190‰ at the onset of woody plant expansion and then decreasing to around −230‰ at 7.0 ka (Fig. 2i).

Alternatively, the changes in $\varepsilon_{hopane/water}$ could reflect changes in microbial metabolism pathways, e.g., with autotrophs generally exhibiting lower $\varepsilon_{lipid/water}$ values than heterotrophs[25,44–47]. Consequently, the observed ~40‰ drop in $\varepsilon_{hopane/water}$ during woody plant expansion could reveal a transient metabolism shift from heterotrophy to greater autotrophy (Supplementary Fig. S5). Differences in biosynthetic pathways add complexity. Bacteria synthesize hopanoids primarily via the methylerythritol phosphate (MEP) pathway, but some heterotrophic bacteria also use the mevalonic acid (MVA) pathway[48]. These pathways generally lead to lower $\varepsilon_{lipid/water}$ values than that of *n*-alkyl lipids synthesized via the acetogenic pathway[47]. Consistent with this, our $\varepsilon_{hopane/water}$ values range from −195‰ to −232‰, with an average of −209‰, which is significantly lower than the $\varepsilon_{lipid/water}$ values of heterotrophic bacterial fatty acids observed in culture (−150‰–+400‰)[25,44]. However, $\varepsilon_{lipid/water}$ values also differ between isoprenoid lipids biosynthesized via the MEP and MVA pathways, with lipids produced through the MEP pathway exhibiting greater fractionation and being more ^{2}H-depleted[26,47,49]. Therefore, the changes in $\varepsilon_{lipid/water}$ (Fig. 2i) likely document a combination of metabolic (i.e., heterotrophy vs autotrophy) and biosynthetic (MEP vs MVA) processes, and understanding of both is limited. Nonetheless, the variation in hopane $\delta^{2}H$ and $\varepsilon_{hopane/water}$ values between 8 to 6 ka, combined with the variation in hopane $\delta^{13}C$ values and the change in hopane abundances and distributions, indicates a dynamic bacterial response to the ZGT vegetation transition.

Microbial metabolism shifts are linked to peat organic composition changes

FTIR spectra reveal peat organic matter composition changes associated with woody plant expansion. Proportions of carbohydrates (related to cellulose and hemi-cellulose) and aromatics (related to lignin and therefore woody tissues) exhibit pronounced fluctuations between 8–6 ka (Fig. 2j, k), corresponding to changes in the relative proportions of woody plants and *Sphagnum* mosses (Fig. 2a). Peaks in woody plant proportions are associated with higher proportions of aromatics ($r = 0.61$, $p = 0.0265$, $n = 13$) and lower proportions of carbohydrates ($r = -0.55$, $p = 0.0534$, $n = 13$) (Supplementary Figs. S6 and S7a, S7b). FTIR spectra also show higher peaks for lignin and aromatic compounds during the woody plant expansion period compared to non-expansion periods (Supplementary Fig. S8). These findings suggest that vegetation shifts drive peat organic matter towards a more recalcitrant[50], aromatic composition during woody plant expansion. This pattern aligns with modern latitudinal trends in peatlands, where tropical and subtropical peatlands, dominated by woody vegetation, show lower carbohydrates and higher aromatic levels than high-latitude peatlands[51]. Intriguingly, the shift towards greater peat aromaticity (and carbohydrate depletion) precedes the woody interval by several thousand years (Fig. 2j, k), likely driven not only by the vegetation changes during early Holocene (Fig. 2a) but also by warming and drying-induced decomposition[52].

The observed changes in peat organic matter recalcitrance during woody plant expansion played a pivotal role in driving bacterial metabolic shifts. Around 7 ka, bacterial $\varepsilon_{hopane/water}$ values decreased by ~40‰, coinciding with a sharp drop in carbohydrates from 40% to 25% and a > 3% rise in aromatics (Fig. 2i, j, k). Correlation analysis reveals that $\varepsilon_{hopane/water}$ values are significantly positively correlated with carbohydrates ($r = 0.67$, $p = 0.0043$, $n = 16$) and significantly negatively correlated with aromatics ($r = -0.64$, $p = 0.008$, $n = 16$) (Supplementary Figs. S6 and S7c, S7d), indicating that higher carbohydrate proportions sustain heterotrophy, while elevated aromatics suppress it. In addition, the $\delta^{13}C$ values of saturated C_{18} fatty acid—likely derived from both fungal and bacterial sources—show similar patterns, with significant positive correlation with carbohydrates ($r = 0.48$, $p = 0.0376$, $n = 19$) and negative correlation with aromatics ($r = -0.56$, $p = 0.0127$, $n = 19$) (Supplementary Figs. S7e, S7f). These relationships suggest that microbes contributing to C_{18} fatty acid production, including fungi, may have adjusted their carbon metabolism in response to peat organic composition changes.

These findings align with broader peatland studies linking increases in organic matter recalcitrance to reduced microbial decomposition and potentially altered metabolism[12,15]. Labile carbohydrates provide energy-rich substrates critical for heterotrophic metabolism, but their decline, driven by woody plant expansion, limited substrate availability and prompted bacterial adaptation toward autotrophy or mixotrophy[53]. Similarly, elevated aromatics, particularly woody litter-derived polyphenols, could have further suppressed heterotrophic metabolism by interfering with microbial enzymatic activity[54,55]. This also explains why we observe no clear trend in bacterial hopanoid abundance, with aerobic conditions that favor bacterial hopanoid-producers countered by organic matter energy limitation. Collectively, our results highlight how woody plant-driven changes in peat organic matter composition constrained microbial heterotrophic metabolism, underscoring the pivotal role of vegetation shifts in regulating peatland microbial dynamics.

Implications for carbon storage in peatlands

Insights into ancient microbial ecology reveal the underlying mechanisms of carbon sequestration during ecological transitions. Total organic carbon (TOC) and apparent carbon accumulation rates (aCAR) significantly increased during the 8–6 ka period, with TOC

https://doi.org/10.1038/s41467-025-62175-1

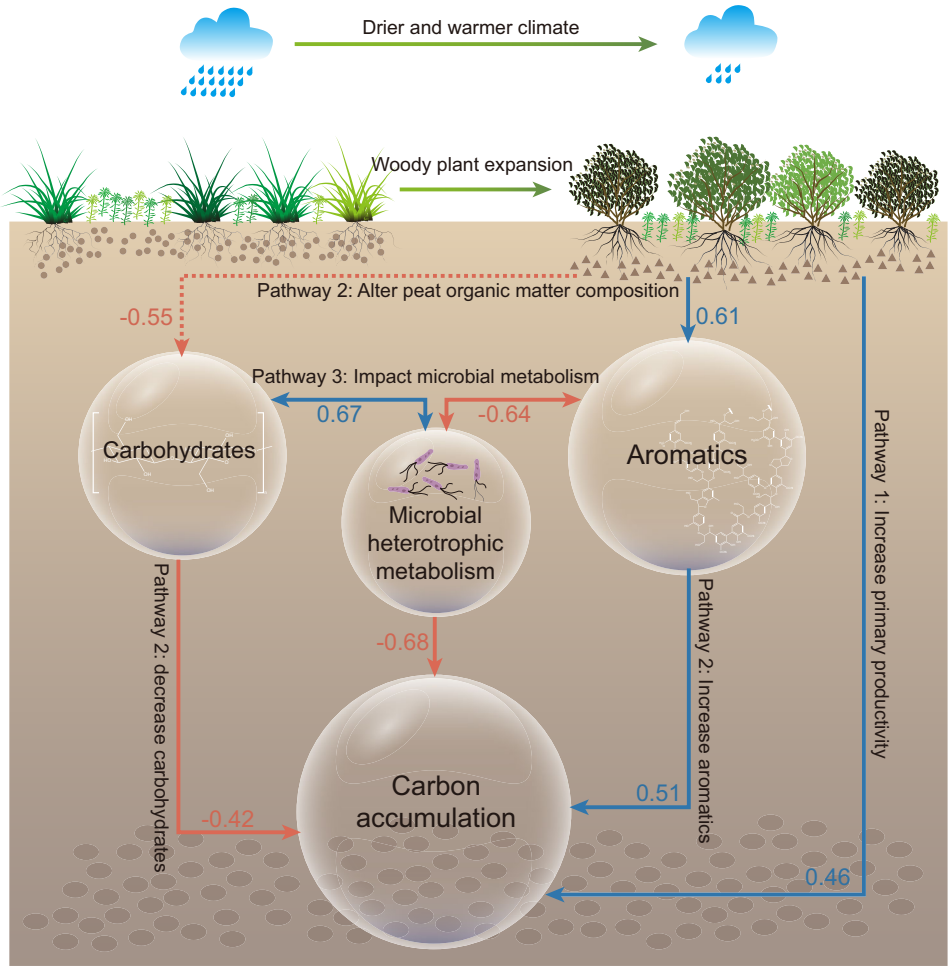

Fig. 3 | Diagram of climate-driven woody plant expansion in peatlands and its effects on peat organic matter composition, microbial metabolism, and carbon accumulation. Three pathways illustrate how woody plant expansion enhances carbon accumulation in peatlands: (1) increasing primary productivity, (2) altering peat organic matter composition by increasing aromatics and reducing carbohydrates, and (3) inhibiting microbial heterotrophic metabolism. Correlation coefficients (r) are shown, with blue arrows indicating positive effects and red arrows indicating negative effects.

rising from 20% to nearly 40% (Fig. 2l), and aCAR increasing from below 40 g C/m^2/yr to a peak of 146 g C/m^2/yr around 7 ka (Fig. 2m). This remarkable increase occurred despite the concurrent warming and drying conditions (Fig. 2b and c), which has been suggested to decrease peatland carbon accumulation through increased organic matter degradation[56]. Because aCAR is derived from peat accumulation rate, TOC, and bulk density, we further examined whether changes in bulk density contributed to the observed aCAR increase. During the 8–6 ka interval, bulk density mostly varies between 0.43 and 0.66 g/cm^3, with a single-point peak at 0.85 g/cm^3 at 7 ka (Fig. 2n), coinciding with the highest aCAR value (Fig. 2m). This alignment suggests that increased compaction may have partially contributed to the aCAR spike. However, bulk density during 8–6 ka is similar to the other periods (Fig. 2n), and even lower than last deglacial values (e.g., 0.8–1.0 g/cm^3 between 14 and 12 ka), indicating that the bulk density cannot explain the high aCAR during 8–6 ka.

We propose that woody plant expansion and the resulting changes in peat organic matter composition and microbial responses have protected peatland carbon storage at the ZGT peatland during periods of warming and drying. Correlation analyses further support this hypothesis, revealing significant relationships between aCAR and woody plant macrofossils, aromatics, carbohydrates, and microbial biomarker $\delta^{13}C$ and $\varepsilon_{hopane/water}$ values (Supplementary Figs. S6 and S7). These findings highlight three key factors that may modulate the climatic impact on carbon accumulation: vegetation, peat organic matter composition, and microbial metabolism.

First, our findings emphasize the well-established central role of vegetation in shaping peatland carbon dynamics (Fig. 3). A positive correlation between woody macrofossil abundance and aCAR ($r = 0.46$, $p = 0.0437$, $n = 20$) (Supplementary Figs. S6 and S7g) suggests that woody plant expansion directly stimulated carbon input (Fig. 3, Pathway 1). This can be attributed to woody-driven enhanced primary productivity, as woody plants can contribute to higher primary productivity through fast-growth root systems and a greater capacity to fix carbon compared to herbaceous vegetation[11,13]. Plant primary productivity has been proposed to play a critical role in determining peatland carbon accumulation over long timescales[17,57], with the capacity to offset carbon losses induced by warming and drying up to a certain point[16].

Second, peat organic matter composition governs its reactivity and therefore carbon accumulation rates (Fig. 3). aCAR in the ZGT peatland exhibits a significant positive correlation with the proportion of aromatics ($r = 0.51$, $p = 0.001$, $n = 38$) and a negative correlation with the proportion of carbohydrates ($r = -0.42$, $p = 0.0083$, $n = 38$) (Supplementary Figs. S6, S7h, S7i), directly linking peat composition to carbon storage. The reduction in labile carbohydrates and increase in recalcitrant aromatics, largely derived from lignin and phenolic compounds in woody residues, indicate a transition toward recalcitrant

organic matter pools (Fig. 3, Pathway 2). These differences, originally set by the dominant peat-forming vegetation, are enhanced by the preferential preservation of the more recalcitrant components; in the ZGT peatland, this affects both the woody interval and the underlying horizons, which could have undergone secondary decomposition during drier periods. Such changes create a chemically stable peat matrix dominated by recalcitrant components[58,59], offering enhanced resistance to degradation and enabling sustained carbon accumulation during mid-Holocene warm and dry conditions.

Finally, the interplay between peat organic matter composition and microbial metabolism further contributes to the resilience of peatland carbon storage (Fig. 3). The significant negative correlation between aCAR and bacterial metabolic $\varepsilon_{hopane/water}$ values ($r = -0.68$, $p = 0.0151$, $n = 12$) highlights the regulatory role of microbial communities on carbon accumulation (Supplementary Figs. S6 and S7j). During the early stages of woody plant expansion under warming and drying conditions, heterotrophic activity increased, as indicated by higher $\varepsilon_{hopane/water}$ values (Fig. 2i). This coincided with an initial rise and subsequent decline in aCAR (Fig. 2m), suggesting that enhanced heterotrophy offset the gains from increased primary productivity, causing aCAR fluctuations. As woody plants expanded further and peat organic matter composition shifted, elevated aromatic and decreased carbohydrate proportions inhibited heterotrophy, facilitating carbon sequestration (Fig. 3, Pathway 3). Notably, the highest aCARs occurred not in intervals with the maximum woody macrofossil abundance but with the lowest $\varepsilon_{hopane/water}$ values and a sharp bacterial and fungal biomass decline around 7.1 ka (Fig. 2d, e, i), emphasizing the critical role of heterotrophic metabolism in shaping carbon storage on top of the influence of plant primary productivity[10,12,15].

Our study suggests that woody plant expansion initiates a cascade of processes—enhanced primary productivity, shifts toward recalcitrant peat organic matter composition, and suppression of microbial heterotrophy—that can collectively drive substantial increases in carbon accumulation and mitigate the typically adverse effects of climate disturbance such as warming and drying, although likely there are limits to how much warming and drying the system may undergo before the peat soils become aerated. Our data allow us to estimate the increased carbon accumulation driven by woody plant expansion at our site. For every 10% increase in the proportion of woody plants, the combined effects of enhanced primary productivity, changes in peat organic matter composition, and shifts in microbial metabolism contribute to an additional 16.9 g C/m^2/yr of carbon accumulation.

However, it is important to recognize that increased woody plant expansion does not necessarily lead to indefinite aCAR increases, as excessive drying can shift peatlands toward aerated conditions, reducing long-term carbon storage. This aligns with growing evidence of a tipping point where further drying no longer enhances carbon accumulation—it has been shown that more dramatic transitions result in greater water table drawdown by evapotranspiration, causing organic carbon oxidation rather than storage[60]. A similar pattern is observed at ZGT peatland, after 6 ka, woody vegetation declined, herbaceous plants resurged (Fig. 2a), and aCAR decreased (Fig. 2m). This pattern may reflect a response to increasingly dry local conditions and/or possible anthropogenic disturbance, although direct evidence remains lacking.

In addition, during the period of woody plant expansion, woody vegetation co-occurred with abundant *Sphagnum* (Fig. 2a), indicating that it remained a peatland rather than completing a full transition to forest. This vegetation balance may have played a crucial role in maintaining peat water levels, preventing excessive drying that could otherwise lead to carbon oxidation. This highlights the critical role of *Sphagnum* in protecting peatland carbon storage through suppressing microbial decomposition[61]. The synergy between *Sphagnum*-derived compounds and woody plant-derived aromatics within a symbiotic ecosystem plays a key role in inhibiting microbial metabolism and promoting the preservation of recalcitrant organic matter, ultimately sustaining long-term carbon accumulation.

Additionally, we propose that aCAR should be interpreted with caution, as it represents the current measured value and may not reflect the original accumulation rate due to post-depositional decomposition and autogenic processes. In our ZGT core, lower aCAR and TOC from the Late Pleistocene to the early Holocene (Fig. 2l, m) were likely influenced in part by enhanced decomposition during later warming and drying, as prolonged exposure in an expanded acrotelm delayed incorporation into the catotelm. This underscores the combined influence of initial carbon inputs and secondary decomposition in shaping aCAR. Consequently, the peak aCAR observed during 8–6 ka may indicate a higher original accumulation rate as well as a more recalcitrant organic matter composition that better resisted degradation during subsequent dry periods. This further highlights the pivotal role of vegetation shifts in shaping peat organic matter composition and microbial activity, ultimately regulating long-term carbon storage.

To broaden the understanding of woody plant impacts on peatland carbon accumulation, we compiled apparent carbon accumulation rate (aCAR) and long-term apparent rate of carbon accumulation (LORCA) data from 155 peatlands globally, comprising 196 peat cores and 520 measurements of aCAR/LORCA (Fig. S9; Supplementary Data 1). To minimize autogenic effects, we excluded aCAR/LORCA data from the recent undecomposed surface layers (acrotelm), which can lead to artificially elevated carbon accumulation estimates. We categorized these aCAR/LORCA records based on vegetation dynamics within these peat cores and climate zones, separating northern peatlands (128 sites, 166 cores, 372 measurements) and tropical peatlands (27 sites, 30 cores, 148 measurements). Within each group, we further distinguished between woody-dominated periods (woody plant proportion > 50%) and non-woody periods. In northern peatlands, the mean aCAR/LORCA during woody-dominated periods was 39.9 g C/m^2/yr ($n = 151$), significantly higher than during non-woody periods (28.1 g C/m^2/yr, $n = 221$; $p < 0.0001$, $t = 4.96$, $df = 370$) (Fig. S9a). In tropical peatlands, the mean aCAR/LORCA during woody-dominated periods was even higher, at 83.1 g C/m^2/yr ($n = 117$), compared to 27.8 g C/m^2/yr during non-woody periods ($n = 31$; $p = 0.0017$, $t = 3.202$, $df = 146$) (Fig. S9b). These findings support a consistent role of woody vegetation in enhancing carbon accumulation across climate zones.

While both tropical and northern peatlands show enhanced aCAR/LORCA during woody-dominated periods, we note that the mean aCAR/LORCA in tropical peatlands is substantially higher (Fig. S9b), despite the high rates of microbial respiration expected at higher temperatures[56]. This likely reflects ecosystem-scale differences in primary productivity, vegetation structure, and peat composition. In particular, tropical swamp forests typically exhibit continuous woody dominance, high litter inputs, and high recalcitrant carbon content[51], all of which may act synergistically to enhance long-term carbon accumulation. Therefore, although woody vegetation appears to support greater aCAR/LORCA across peatland types, the underlying mechanisms may differ between tropical and northern systems.

Further comparisons of Holocene carbon accumulation and net carbon pool data from 127 northern peatland sites, alongside woody macrofossil records from 76 sites[23,62,63] indicate that continuous woody plant expansion in those settings is also closely linked to increased carbon pools and aCAR (Fig. S9). Notably, accelerated woody expansion in the past 2000 years has likely driven substantial increases in both net carbon pools and aCAR (Figs. S9c, S9d, S9e), although caution should be taken when comparing recent aCAR due to the autogenic effect of the partially undecomposed acrotelm resulting in apparently higher aCAR[64,65] that do not necessarily result in higher long-term accumulation.

This more extensive dataset reinforces the idea that woody plant expansion may have a favorable impact on peatland carbon

accumulation on a millennial scale, highlighting its importance in maintaining peatland carbon storage amid climatic shifts. Our findings emphasize the crucial interactions between plants, peat organic matter composition, and microbial processes that enable at least some peatlands to sustain long-term carbon storage through the expansion of woody plants. As ecosystems are reshaped by climate change, woody plant expansion offers a promising natural strategy to bolster peatland resilience and enhance carbon sequestration. However, the effectiveness of this feedback will depend on the adaptive responses of microbial communities, stability of hydrological systems, and extent of the woody plant expansion. By integrating past peatland dynamics with future projections, our study underscores the need to understand and harness these mechanisms to maximize the role of peatlands as effective long-term carbon sinks in mitigating global climate change.

Methods

Study site

The ZGT peatland (26°24′40″N, 114°04′40″E) is a mire located in Yanling County, Hunan Province, at an elevation of 1600–1800 m above sea level. It is surrounded by peaks ranging from 1790 to 1830 m and lies at the headwaters of a local stream. The regional vegetation is dominated by evergreen broadleaved forests, while the peatland itself features a mix of shrubs (*Camellia caudata*, *Rhododendron spp.*), sedges (*Carex spp.*), and mosses (*Sphagnum palustre*, *Polytrichum commune*) (Fig. 1). The site experiences a mean annual temperature of 14.2 °C and a mean annual precipitation of 1890 mm[66].

Three 2-m peat cores were collected in September 2016 using a Russian peat corer in the central area of the ZGT peatland. The cores revealed a surface layer of plant remains, underlain by black humified peat (4–26 cm) and brown peat (26–184 cm). Below 184 cm, the peat transitions to gravelly sediments over granite bedrock[35]. The peat cores were subsampled at 1 cm intervals in the field, then transported to the laboratory and stored at −20 °C prior to any further processing.

Radiocarbon dating

Radiocarbon dating was performed on 19 selected peat samples, with plant macrofossils such as leaves, seeds, and shoots carefully examined under a microscope prior to analysis. The prepared samples were sent to Beta Analytic Inc. for radiocarbon measurements. The resulting conventional radiocarbon ages were calibrated to calendar years using the Bacon age-depth model. The results indicate that the 184 cm peat core spans the past 14,000 years (Supplementary Fig. S10)[35].

Plant macrofossil analysis

Plant macrofossil analysis and identification were conducted following standard protocol[20]. Briefly, 2 cm^3 peat subsamples were treated using a NaOH extraction method. Each subsample was placed in a 100 ml beaker with 5% NaOH solution, heated to boiling, and maintained for 2 hours to remove humic acids that could interfere with microscopic observation. After cooling, the samples were passed through a 125 μm sieve and rinsed thoroughly with distilled water until the filtrate was clear, leaving only plant residues on the sieve. The cleaned residues were transferred with tweezers into labeled centrifuge tubes containing deionized water for further analysis. Plant macrofossil identification was performed using the Quadrat and Leaf Count Macrofossil Analysis (QLCMA) method. The centrifuge tubes were gently shaken, and small amounts of residue were transferred to Petri dishes overlaid with a 10×10 grid. Under a stereo microscope (10× to 50× magnification), residues were examined across 20 randomly selected fields of view. Remaining residues were subsequently analyzed in additional Petri dishes until all materials had been examined. The relative abundance of woody, herbaceous, and moss remains was calculated as percentages of the total macrofossil content.

Lipid extraction and instrumental analysis

Approximately 1.5 g of freeze-dried peat was finely ground to pass through a 60-mesh sieve. The lipids were extracted by sonicating the sample six times for 10 min each using a dichloromethane/methanol mixture (9:1, v/v). An internal standard of androstane, androstanol, and cholanic acid were added prior to extraction. Solvent was removed using a rotary evaporator under reduced pressure, and the resulting extract was fractionated through silica gel column chromatography. Sequential elution with hexane, hexane/dichloromethane (1:1, v/v), and dichloromethane/methanol (1:1, v/v) yielded aliphatic, aromatic, and polar fractions. The aliphatic fraction was analyzed with a gas chromatograph-mass spectrometer (GC-MS; Agilent 6890 GC interfaced with a 5973 mass selective detector) equipped with a DB-5MS column (30 m × 0.25 mm, 0.25 μm film thickness). The GC oven was programmed to start at 70 °C (1 min hold), ramp to 200 °C at 10 °C/min, and then to 300 °C at 3 °C/min (10 min hold). The polar fraction was subjected to saponification to separate it into neutral and acidic sub-fractions. The acidic sub-fraction was then methylated using BF_3-methanol to produce fatty acid methyl esters (FAMEs), which were subsequently analyzed using the same instrumentation and protocols as described above.

Compound-specific carbon isotope ratios ($\delta^{13}C$) were determined using a Finnigan Trace GC connected to a Delta Plus XP isotope ratio mass spectrometer with a DB-5MS column (60 m × 0.25 mm, 0.25 μm film thickness). The oven program began at 50 °C (1 min hold), ramped to 220 °C at 10 °C/min (2 min hold), then to 300 °C at 2 °C/min, and finally to 310 °C at 10 °C/min (20 min hold). For $\delta^{13}C$ analysis, the oxidation furnace was maintained at 950 °C. Squalane ($\delta^{13}C = -19.8‰$) was used as the internal standard, and system calibration was carried out using *n*-alkane standards (C_{16}-C_{30}, Indiana University). Carbon isotope reproducibility was better than ±0.5‰. For hydrogen isotope ratios (δ^2H), a Finnigan Trace GC coupled to a Delta V Advantage mass spectrometer was used, with a high-temperature conversion furnace at 1400 °C. Squalane ($\delta^2H = -167‰$) served as the internal standard, and calibration was verified using *n*-alkane standards with known δ^2H values (Indiana University). Reproducibility for δ^2H measurements was better than ±5‰. Peak amplitudes were maintained within 1–4 V for δ^2H and 0.5–4 V for $\delta^{13}C$ to ensure data quality, with results discarded for peaks below these thresholds. All isotope results were reported in delta notation (‰) relative to VSMOW for δ^2H and VPDB for $\delta^{13}C$. To correct for the isotopic contribution of the added methyl group during methylation, we applied a mass balance correction using the following equation:

$$\delta^{13}C_{FA} = [(n+1) \times \delta^{13}C_{FAME} - \delta^{13}C_{methanol}]/n \quad (1)$$

where n is the number of carbon atoms in the fatty acid, $\delta^{13}C_{FAME}$ is the measured isotopic composition of the fatty acid methyl ester, and $\delta^{13}C_{methanol}$ is the $\delta^{13}C$ value of the methanol used for methylation. The $\delta^{13}C_{methanol}$ was determined by methylating phthalic acid of known isotopic composition (reference standard provided by Dr. Arndt Schimmelmann, Indiana University) and calculating the value based on mass balance.

Isotope offset calculation

The isotopic offset for carbon and hydrogen between $C_{31}\alpha\beta$ hopane and their respective reference materials was determined using the following equations:

$$\varepsilon_{hopane/bulk} = \frac{\delta^{13}C_{hopane} + 1}{\delta^{13}C_{bulk} + 1} - 1 \quad (2)$$

$$\varepsilon_{hopane/water} = \frac{\delta^{2}H_{hopane} + 1}{\delta^{2}H_{water} + 1} - 1 \quad (3)$$

The calculated offsets were scaled by a factor of 1000 and expressed in per mil (‰) following standard reporting conventions[48]. Here, the $\delta^{13}C_{bulk}$ represents the bulk organic carbon isotopic composition of the peat, and $\delta^{2}H_{water}$ denotes the isotopic composition of precipitation water. The $\delta^{2}H_{water}$ values were estimated using the regional meteoric water line and calculated based on the oxygen isotopic composition of carbonate from nearby Dongge Cave, as described by the equation:

$$\delta^{2}H_{water} = 7.9 \times \delta^{18}O_{carb} + 8.2 \quad (4)$$

Where the $\delta^{18}O_{carb}$ is the carbonate oxygen isotope value derived from the Dongge Cave[67], assumed to represent the regional precipitation oxygen isotope composition. Effects of temperature on precipitation $\delta^{18}O$ and on fractionation during carbonate formation were considered negligible, as the temperature dependence of oxygen isotope fractionation have minimal (+0.05‰/°C) impact under southern China's climatic conditions, and the slope (7.9) and intercept (8.2) correspond to the regional meteoric water line parameters[33].

Fourier transform infrared (FTIR) spectroscopy

FTIR spectroscopy was used to analyze the chemical components of peat organic matter[51,68]. Briefly, the FTIR spectra were obtained using an ALPHA II spectrometer (Bruker, Germany) with KBr pellets prepared by mixing 150 mg of dried KBr with 1 mg of finely ground peat sample. Spectra were acquired over the range of 4000–450 cm^{-1} at a resolution of 1 cm^{-1}, and baseline corrections were applied to ensure accuracy. A total of 32 scans were averaged for each sample. Key peaks in the spectra were selected to quantify carbohydrates and aromatics (Supplementary Fig. S8), carbohydrates were assessed from the carb peak (1030–1080 cm^{-1}), while aromatics were represented by arom15 (1513–1515 cm^{-1}) and arom16 (1600–1650 cm^{-1})[51]. Peak heights were normalized to the total spectral area[51], to allow for consistent cross-sample comparisons. The ratios of these normalized peak areas were used to evaluate the peat organic matter composition alterations in the ZGT peat core.

Carbon dynamics and bulk geochemical analysis

The total organic carbon content of the peat samples was determined using a Vario MiCRO cube Element Analyzer. Dry bulk density was measured by determining the mass of peat dried at 50 °C and dividing it by the known sample volume. The apparent carbon accumulation rate (aCAR, g C/m^2/yr) was calculated using the following equation[69]:

$$aCAR = r/1000 \times \tilde{n} \times c \quad (5)$$

where r represents the peat accumulation rate (mm/yr), $\tilde{n}$ is the dry bulk density (g/m^3), and c is the carbon content (g C/g dry weight).

The $\delta^{13}C_{bulk}$ of peat organic carbon were analyzed using an elemental analyzer coupled to a Finnigan MAT253 isotope ratio mass spectrometer. Prior to analysis, freeze-dried samples were finely ground and sieved through a 200-mesh sieve to ensure uniformity. To remove carbonates, samples were treated with HCl, followed by a secondary freeze-drying step. Approximately 40–60 mg of the treated sample was encapsulated in tin cups for analysis. Calibration of the $\delta^{13}C$ values of bulk organic carbon was conducted using certified reference materials of GBW04407 ($\delta^{13}C = -22.4‰$) and GBW04408 ($\delta^{13}C = -36.9‰$). A replicate was analyzed every six samples to monitor consistency, with a reproducibility better than ±0.2‰. A blank correction was applied by analyzing empty tin cups to account for background signals. To ensure consistent peak amplitudes, injection volumes were carefully controlled so that sample signals matched those of the calibration standards.

Global data collection

We compiled carbon accumulation data from 196 peat cores across 155 peatlands worldwide. These data include a total of 520 measurements of apparent carbon accumulation rates (aCAR) and long-term apparent carbon accumulation rates (LORCA). Peatland site information and data sources are provided in the Supplementary Data 1. To avoid overestimation of long-term carbon accumulation, we excluded the significantly elevated aCAR values observed in the uppermost layers of peat cores. These elevated rates are likely influenced by the recent accumulation of undecomposed organic matter that has not undergone secondary decomposition processes. In other words, the autogenic effects of partially undecomposed surface layers (acrotelm) can lead to artificially high aCAR values, but this does not necessarily indicate greater long-term carbon accumulation.

To account for ecological differences between climatic zones, we categorized the compiled aCAR/LORCA records into two groups: northern peatlands and tropical peatlands. Northern peatlands include 128 sites with 166 cores and 372 measurements of aCAR/LORCA, while tropical peatlands include 27 sites with 30 cores and 148 measurements. This separation was made given that tropical swamps are ecologically distinct from northern peatland systems. Within each group, we categorized the carbon accumulation data into woody-dominated and non-woody-dominated periods based on vegetation reconstructions from the same peat cores. A period was classified as woody-dominated when woody plants (including shrubs and trees) accounted for more than 50% of the plant community. For peat cores lacking vegetation reconstructions, classification was based on the overall description of plant remains within the core, peat lithology (e.g., woody peat vs. herbaceous peat), and the modern vegetation composition at the site.

Statistical analyses

All statistical analyses were conducted to assess relationships and differences among variables. For correlation analyses, Pearson correlation coefficients (r) were calculated, and results were reported with significance (p values) and sample size (n). For comparisons between two groups, an unpaired t-test was used to assess significant differences, with results expressed as p-value, t-value, degrees of freedom (df), and sample size (n). For comparisons among three or more groups, such as isotopic differences in n-alkanes among herbaceous plants, woody plants, and *Sphagnum* mosses (Fig. S2), one-way ANOVA was performed. Results were reported with p-value, F-value, degrees of freedom (df), and sample size (n). The significance threshold was set at $p = 0.05$. We also applied the coefficient of variation, variance, and subsampling to verify that the increased variability during the 8–6 ka period was not an artifact of a higher number of data points. When sample sizes were equalized, both the coefficient of variation and variance remained higher during 8–6 ka compared to other periods, confirming the robustness of this pattern.

Data availability

All data supporting this study are provided in the Supplementary Data 1 file and Figshare data repository (https://doi.org/10.6084/m9.figshare.29484650).

References

1. Yu, Z. et al. Global peatland dynamics since the Last Glacial Maximum. *Geophys. Res. Lett.* **37**, L13402 (2010).
2. Xu, J., Morris, P. J., Liu, J. & Holden, J. PEATMAP: refining estimates of global peatland distribution based on a meta-analysis. *Catena*. **160**, 134–140 (2018).
3. Loisel, J. et al. Insights and issues with estimating northern peatland carbon stocks and fluxes since the Last Glacial Maximum. *Earth Sci. Rev.* **165**, 59–80 (2017).

4. Morris, P. J. et al. Global peatland initiation driven by regionally asynchronous warming. *Proc. Natl. Acad. Sci. USA.* **115**, 4851–4856 (2018).
5. Treat, C. C. et al. Widespread global peatland establishment and persistence over the last 130,000 years. *Proc. Natl. Acad. Sci. USA.* **116**, 4822–4827 (2019).
6. Bragazza, L. et al. Biogeochemical plant–soil microbe feedback in response to climate warming in peatlands. *Nat. Clim. Change* **3**, 273–277 (2013).
7. Holmgren, M. et al. Positive shrub–tree interactions facilitate woody encroachment in boreal peatlands. *J. Ecol.* **103**, 58–66 (2015).
8. Swindles, G. T. et al. Ecosystem state shifts during long-term development of an Amazonian peatland. *Glob. Chang. Biol.* **24**, 738–757 (2018).
9. Limpens, J. et al. Shrubs and degraded permafrost pave the way for tree establishment in subarctic peatlands. *Ecosystems* **24**, 370–383 (2021).
10. Buttler, A. et al. Ericoid shrub encroachment shifts aboveground–belowground linkages in three peatlands across Europe and Western Siberia. *Glob. Chang. Biol.* **29**, 6772–6793 (2023).
11. Malhotra, A. et al. Peatland warming strongly increases fine-root growth. *Proc. Natl. Acad. Sci. USA.* **117**, 17627–17634 (2020).
12. Fenner, N. & Freeman, C. Woody litter protects peat carbon stocks during drought. *Nat. Clim. Change* **10**, 363–369 (2020).
13. Walker, T. N. et al. Vascular plants promote ancient peatland carbon loss with climate warming. *Glob. Chang. Biol.* **22**, 1880–1889 (2016).
14. Xue, W. et al. From Sphagnum to shrub: Increased acidity reduces peat bacterial diversity and keystone microbial taxa imply peatland degradation. *Land Degrad. Dev.* **34**, 5259–5272 (2023).
15. Wang, H. et al. Vegetation and microbes interact to preserve carbon in many wooded peatlands. *Commun. Earth Environ.* **2**, 67 (2021).
16. Gallego-Sala, A. V. et al. Latitudinal limits to the predicted increase of the peatland carbon sink with warming. *Nat. Clim. Change* **8**, 907–913 (2018).
17. Charman, D. J. et al. Climate-related changes in peatland carbon accumulation during the last millennium. *Biogeosciences* **10**, 929–944 (2013).
18. Loisel, J. et al. Expert assessment of future vulnerability of the global peatland carbon sink. *Nat. Clim. Change* **11**, 70–77 (2021).
19. Zhao, Y. et al. Plant–microbe interactions underpin contrasting enzymatic responses to wetland drainage. *Nat. Clim. Chang.* **14**, 1078–1086 (2024).
20. Mauquoy, D., Hughes, P. D. M. & Van Geel, B. A protocol for plant macrofossil analysis of peat deposits. *Mires Peat.* **7**, 1–5 (2010).
21. Gałka, M. et al. Response of plant communities to climate change during the late Holocene: Palaeoecological insights from peatlands in the Alaskan Arctic. *Ecol. Indic.* **85**, 525–536 (2018).
22. Sim, T. G. et al. Pathways for ecological change in Canadian High Arctic wetlands under rapid twentieth century warming. *Geophys. Res. Lett.* **46**, 4726–4737 (2019).
23. Fewster, R. E. et al. Holocene vegetation dynamics of circum-Arctic permafrost peatlands. *Quat. Sci. Rev.* **307**, 108055 (2023).
24. Inglis, G. N. et al. $\delta^{13}C$ values of bacterial hopanoids and leaf waxes as tracers for methanotrophy in peatlands. *Geochim. Cosmochim. Acta* **260**, 244–256 (2019).
25. Wijker, R. S. et al. $^{2}H/^{1}H$ variation in microbial lipids is controlled by NADPH metabolism. *Proc. Natl. Acad. Sci. USA.* **116**, 12173–12182 (2019).
26. Pancost, R. D. Biomarker carbon and hydrogen isotopes reveal changing peatland vegetation, hydroclimate and biogeochemical tipping points. *Quat. Sci. Rev.* **339**, 108828 (2024).
27. Zhang, Y. et al. The stable carbon and hydrogen isotopic composition of microbial fatty acids traces microbial metabolism in soils and peats. *Geochim. Cosmochim. Acta.* **365**, 85–100 (2024).
28. Wang, M. et al. Branched GDGT-based paleotemperature reconstruction of the last 30,000 years in humid monsoon region of Southeast China. *Chem. Geol.* **463**, 94–102 (2017).
29. Li, Q. et al. Coupled temperature variations in the Huguangyan Maar Lake between high and low latitude. *Quat. Sci. Rev.* **305**, 108011 (2023).
30. Kaufman, D. et al. A global database of Holocene paleotemperature records. *Sci. Data* **7**, 1–34 (2020).
31. Raghoebarsing, A. A. et al. Methanotrophic symbionts provide carbon for photosynthesis in peat bogs. *Nature* **436**, 1153–1156 (2005).
32. Nichols, J. E., Isles, P. D. F. & Peteet, D. M. A novel framework for quantifying past methane recycling by *Sphagnum*-methanotroph symbiosis using carbon and hydrogen isotope ratios of leaf wax biomarkers. *Geochem. Geophys. Geosyst.* **15**, 1827–1836 (2014).
33. Huang, X. et al. Response of carbon cycle to drier conditions in the mid-Holocene in central China. *Nat. Commun.* **9**, 1369 (2018).
34. McFarlin, J. M. et al. Aquatic plant wax hydrogen and carbon isotopes in Greenland lakes record shifts in methane cycling during past Holocene warming. *Sci. Adv.* **9**, eadh9704 (2023).
35. Huang, X. et al. Holocene forcing of East Asian hydroclimate recorded in a subtropical peatland from southeastern China. *Clim. Dyn.* **60**, 981–993 (2023).
36. Xie, S. et al. Concordant monsoon-driven postglacial hydrological changes in peat and stalagmite records and their impacts on prehistoric cultures in central China. *Geology* **41**, 827–830 (2013).
37. Laiho, R. et al. Dynamics of plant-mediated organic matter and nutrient cycling following water-level drawdown in boreal peatlands. *Glob. Biogeochem. Cycles* **17**, 1053 (2003).
38. Heijmans, M. M. P. D. et al. Persistent versus transient tree encroachment of temperate peat bogs: effects of climate warming and drought events. *Glob. Change Biol.* **19**, 2240–2250 (2013).
39. Moore, P. A. et al. Examining the peatland shrubification-evapotranspiration feedback following multi-decadal water table manipulation. *Hydrol. Process.* **36**, e14719 (2022).
40. Pancost, R. D., Baas, M., van Geel, B. & Sinninghe Damsté, J. S. Response of an ombrotrophic bog to a regional climate event revealed by macrofossil, molecular and carbon isotopic data. *Holocene* **13**, 921–932 (2003).
41. Bragazza, L., Bardgett, R. D., Mitchell, E. A. & Buttler, A. Linking soil microbial communities to vascular plant abundance along a climate gradient. *New Phytol.* **205**, 1175–1182 (2015).
42. Pancost, R. D. & Sinninghe Damsté, J. S. Carbon isotopic compositions of prokaryotic lipids as tracers of carbon cycling in diverse settings. *Chem. Geol.* **195**, 29–58 (2003).
43. Londry, K. L. et al. Stable carbon isotope fractionation between substrates and products of *Methanosarcina barkeri*. *Org. Geochem.* **39**, 608–621 (2008).
44. Zhang, X., Gillespie, A. L. & Sessions, A. L. Large D/H variations in bacterial lipids reflect central metabolic pathways. *Proc. Natl. Acad. Sci. USA.* **106**, 12580–12586 (2009).
45. Osburn, M. R. et al. Fractionation of hydrogen isotopes by sulfate- and nitrate-reducing bacteria. *Front. Microbiol.* **7**, 1166 (2016).
46. Leavitt, W. D. et al. Controls on the hydrogen isotope composition of tetraether lipids in an autotrophic ammonia-oxidizing marine archaeon. *Geochim. Cosmochim. Acta.* **352**, 194–210 (2023).
47. Rhim, J. H. et al. Metabolic imprints in the hydrogen isotopes of *Archaeoglobus fulgidus* tetraether lipids. *Geochim. Cosmochim. Acta* **386**, 196–212 (2024).
48. Sachse, D. et al. Molecular paleohydrology: interpreting the hydrogen-isotopic composition of lipid biomarkers from photosynthesizing organisms. *Annu. Rev. Earth Planet. Sci.* **40**, 221–249 (2012).
49. Ladd, S. N. et al. Metabolic exchange between pathways for isoprenoid synthesis and implications for biosynthetic hydrogen isotope fractionation. *New Phytol.* **231**, 1708–1719 (2021).

50. Normand, A. et al. Organic matter chemistry drives carbon dioxide production of peatlands. *Geophys. Res. Lett.* **48**, e2021GL093392 (2021).
51. Hodgkins, S. B. et al. Tropical peatland carbon storage linked to global latitudinal trends in peat recalcitrance. *Nat. Commun.* **9**, 3640 (2018).
52. Wilson, R. M. et al. Soil metabolome response to whole-ecosystem warming at the Spruce and Peatland Responses under Changing Environments experiment. *Proc. Natl. Acad. Sci. USA*. **118**, e2004192118 (2021).
53. Qin, L. et al. Changes in bacterial communities during rice cultivation remove phenolic constraints on peatland carbon preservation. *ISME Commun.* **4**, ycae022 (2024).
54. Fenner, N. & Freeman, C. Drought-induced carbon loss in peatlands. *Nat. Geosci.* **4**, 895–900 (2011).
55. Wang, H., Richardson, C. J. & Ho, M. Dual controls on carbon loss during drought in peatlands. *Nat. Clim. Change* **5**, 584–587 (2015).
56. Dorrepaal, E. et al. Carbon respiration from subsurface peat accelerated by climate warming in the subarctic. *Nature* **460**, 616–619 (2009).
57. Beilman, D. W., MacDonald, G. M., Smith, L. C. & Reimer, P. J. Carbon accumulation in peatlands of West Siberia over the last 2000 years. *Glob. Biogeochem. Cycles* **23**, 1 (2009).
58. Leifeld, J., Steffens, M. & Galego-Sala, A. Sensitivity of peatland carbon loss to organic matter quality. *Geophys. Res. Lett.* **39**, 14 (2012).
59. Martínez Cortizas, A. et al. 9000 years of changes in peat organic matter composition in Store Mosse (Sweden) traced using FTIR-ATR. *Boreas*. **50**, 1161–1178 (2021).
60. Garcin, Y. et al. Hydroclimatic vulnerability of peat carbon in the central Congo Basin. *Nature* **612**, 277–282 (2022).
61. Zhao, Y. et al. *Sphagnum* increases soil's sequestration capacity of mineral-associated organic carbon via activating metal oxides. *Nat. Commun.* **14**, 5052 (2023).
62. Yu, Z. Northern peatland carbon stocks and dynamics: a review. *Biogeosciences* **9**, 4071–4085 (2012).
63. Loisel, J. et al. A database and synthesis of northern peatland soil properties and Holocene carbon and nitrogen accumulation. *Holocene*. **24**, 1028–1042 (2014).
64. Young, D. M. et al. Misinterpreting carbon accumulation rates in records from near-surface peat. *Sci. Rep.* **9**, 17939 (2019).
65. Young, D. M. et al. A cautionary tale about using the apparent carbon accumulation rate (aCAR) obtained from peat cores. *Sci. Rep.* **11**, 9547 (2021).
66. Han, A. et al. Holocene climate records from a mountain wetland in the Luoxiao Ranges. *Trop. Geogr.* **36**, 477–485, 520 (2016). (in Chinese with English abstract).
67. Dykoski, C. A. et al. A high-resolution, absolute-dated Holocene and deglacial Asian monsoon record from Dongge Cave, China. *Earth Planet. Sci. Lett.* **233**, 71–86 (2005).
68. Gao, C. et al. High intensity fire accelerates accumulation of a stable carbon pool in permafrost peatlands under climate warming. *Catena*. **227**, 107108 (2023).
69. Tolonen, K. & Turunen, J. Accumulation rates of carbon in mires in Finland and implications for climate change. *Holocene*. **6**, 171–178 (1996).

Acknowledgements

We thank Dr. Chuanyu Gao from the Northeast Institute of Geography and Agroecology, Chinese Academy of Sciences, for his assistance in FTIR analysis. We thank Dr. Junwu Shu, Dr Yang Yang, Xin Yang, Jiping Cao, Guang Yang and Amutiebu for their help in the field work. This work was supported by the National Natural Science Foundation of China (grants 42293290 to S.X., U20A2094 to X.H., 42402314 to Y.Z.), the 111 Program (National Bureau for Foreign Experts and Ministry of Education of China; grant BP0820004 to S.X.) and the China Postdoctoral Science Foundation (grant 2022M722937 to Y.Z.). R.D.P. acknowledges funding from UK Research and Innovation (UKRI) under the UK government's Horizon Europe funding guarantee [CERES EP/X023214/1] and the Leverhulme Trust.

Author contributions

X.H. and S.X. designed the study. B.Z. and X.H. collected samples. B.Z., C.Y., Y.Z., H-Y.Z., H-B.Z. and X.H. performed laboratory work and instrumental measurements. Y.Z. and X.H. analyzed the data. Y.Z. and X.H. wrote the manuscript with contributions from T.A.H., R.H.P., M.V., A.V.G., R.D.P. and S.X. All authors contributed to the data interpretation and discussion.

Competing interests

The authors declare no competing interests.

Additional information

Supplementary information The online version contains supplementary material available at https://doi.org/10.1038/s41467-025-62175-1.

Correspondence and requests for materials should be addressed to Xianyu Huang.

Peer review information *Nature Communications* thanks Miriam Gross-Schmölders and Zicheng Yu for their contribution to the peer review of this work. A peer review file is available.